ACS APPLIED ENERGY MATERIALS
Cite This: ACS Appl. Energy Mater. XXXX, XXX, XXX−XXX
Article
www.acsaem.org

Dynamics of Photoinduced Degradation of Perovskite Photovoltaics: From Reversible to Irreversible Processes

Mark V. Khenkin,[†] Anoop K. M.,[†] Iris Visoly-Fisher,[†,‡] Sofiya Kolusheva,[‡] Yulia Galagan,[§] Francesco Di Giacomo,[§] Olivera Vukovic,[§] Bhushan Ramesh Patil,[∥] Golnaz Sherafatipour,[∥] Vida Turkovic,[∥] Horst-Günter Rubahn,[∥] Morten Madsen,[∥] Alexander V. Mazanik,[⊥] and Eugene A. Katz*[,†,‡]

[†]Department of Solar Energy and Environmental Physics, Swiss Institute for Dryland Environmental and Energy Research, Jacob Blaustein Institutes for Desert Research, Ben-Gurion University of the Negev, Midreshet Ben-Gurion 8499000, Israel

[‡]Ilse Katz Institute for Nanoscale Science and Technology, Ben-Gurion University of the Negev, Be'er-Sheva 8410501, Israel

[§]Holst Centre, Solliance, High Tech Campus 21, 5656 AE, Eindhoven, The Netherlands

[∥]SDU NanoSYD, Mads Clausen Institute, University of Southern Denmark, Alsion 2, DK-6400 Sønderborg, Denmark

[⊥]Energy Physics Department, Belarusian State University, 4, Nezavisimosti Avenue, 220030 Minsk, Republic of Belarus

Supporting Information

ABSTRACT: The operational stability of perovskite solar cells (PSCs) remains a limiting factor in their commercial implementation. We studied the long-term outdoor stability of ITO/SnO_2/$Cs_{0.05}((CH_3NH_3)_{0.15}(CH(NH_2)_2)_{0.85})_{0.95}PbI_{2.55}Br_{0.45}$/spiro-OMeTAD/Au cells, as well as the dynamics of their degradation, under simulated sunlight indoors and their recovery in the dark. The extent of overall degradation was found to depend on processes occurring both under illumination and in the dark, i.e., during the daytime and nighttime, with the dynamics varying with cell aging. Full recovery of efficiency in the dark was observed for cells at early degradation stages. Further cell degradation resulted in recovery times much longer than one night, appearing as irreversible degradation under real operational conditions. At later degradation stages, very different dynamics were observed: short-circuit current density and fill factor exhibited a pronounced drop upon light turn-off but strong improvement under subsequent illumination. The interplay of reversible and irreversible degradation processes with different recovery dynamics was demonstrated to result in changes in the cell's diurnal PCE dependence during its operational lifespan under real sunlight conditions.

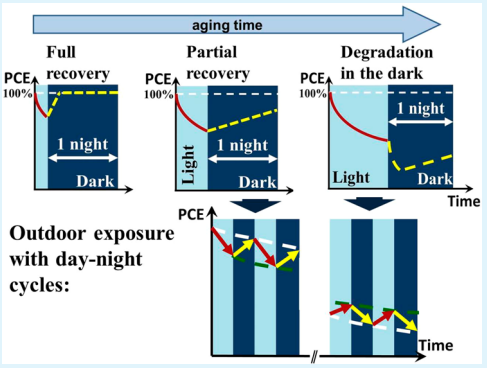

KEYWORDS: *perovskite solar cells, stability, reversible and irreversible degradation, light soaking, recovery dynamics*

1. INTRODUCTION

Hybrid organic−inorganic metal halide perovskite solar cells (PSCs) have already reached power conversion efficiency (PCE) above 22%[1] for laboratory scale cells and over 12%[2] and 10%[3] for large area cells and modules, respectively. However, development of devices combining high PCE and operational stability remains challenging. Numerous studies have addressed the instability of perovskite and transport layers in PSCs induced by heat,[4−6] visible[7] and UV light,[8,9] electric field,[10,11] and exposure to moisture and oxygen.[12] In real operational outdoor conditions, many of these factors affect the cell simultaneously, causing superimposed degradation mechanisms. The complexity of analyzing results may be one of the reasons why outdoor PSC stability data are still rather limited.[13,14]

Recently, attention has been drawn to the reversibility of certain PSC degradation processes.[15−18] During recovery in the dark, the loss in device performance under previous light exposure can be fully or partially compensated. Reversible performance improvement under illumination and subsequent degradation in the dark were also reported for some PSCs.[9,19,20] Such behavior, which is often referred to as the "light soaking effect", was mostly attributed to trap filling processes upon illumination. Huang et al. showed that the time needed for performance recovery under illumination increases with each successive illumination−darkness cycle, demonstrating an interplay between different mechanisms; the term "fatigue" was used to describe this behavior.[19]

Natural sunlight's diurnal cycle has a dark period, during which the cell may undergo recovery processes. We previously used outdoor exposure to natural sunlight to demonstrate these two types of PCE dynamics in different PSCs:[21] "degradation during the day−recovery during the night" and "degradation during the

Received: December 12, 2017
Accepted: January 29, 2018
Published: January 29, 2018

DOI: 10.1021/acsaem.7b00256
ACS Appl. Energy Mater. XXXX, XXX, XXX−XXX

night−recovery during the day", referred to below as "type I" and "type II" diurnal behaviors, respectively. Furthermore, we have shown that the diurnal behavior of type I can be changed into type II at certain aging stages. In the present study of similar planar PSCs, in which the perovskite contains mixed A-cations and mixed halides, we focus on the dynamics of degradation and recovery processes under light−dark exposure. We relate the degradation and recovery dynamics observed by indoor measurements under constant illumination with those observed in outdoor studies under natural sunlight and day−night cycling. This allows us to suggest degradation mechanisms that may be responsible for both types of diurnal behaviors.

This work is organized in the following way: the description of experimental methods is followed by the presentation of PSC recovery kinetics in the dark after degradation to different extents under constant illumination. Then possible underlying degradation mechanisms, responsible for different degradation−recovery dynamics, are discussed. Finally, we show, through outdoor stability testing, how the interplay of these processes explains the noted changes in the cell's diurnal PCE behavior during its lifespan.

2. MATERIALS AND METHODS

2.1. Cell Preparation and Testing. Glass substrates of 3 cm × 3 cm with patterned ITO electrodes were purchased from Naranjo. The substrates were cleaned by sequential sonication in a detergent solution, deionized water, and isopropanol and finally treated with UV−O_3 for 30 min.

A tin oxide (SnO_2) nanoparticle solution (15 wt %), purchased from Alfa Aesar, was diluted by ultrapure water in a volume ratio of 1:5. The ink was spin-coated at a spin speed of 2800 rpm for 50 s and annealed for 30 min at 150 °C. The SnO_2 layer's thickness was 30−40 nm. After preparing SnO_2, samples were transferred to a N_2-filled glovebox for the perovskite deposition.

Next, 1.3 mM lead iodide (PbI_2; TCI) and 1.17 mM formamidinium iodide (FAI, in which FA = $CH(NH_2)_2$; Greatcell Solar) were dissolved in 1 mL of *N*,*N*-dimethylformamide (DMF): dimethyl sulfoxide (DMSO) solution (volume ratio of 9:1). Then, 1.3 mM lead bromide ($PbBr_2$; TCI) and 1.3 mM methylammonium bromide (MABr, in which MA = CH_3NH_3; Greatcell Solar) were dissolved in 1 mL of DMF:DMSO solution (volume ratio of 9:1). Cesium iodide (CsI; Sigma-Aldrich) was dissolved in pure DMSO, adding 1.5 mM to 1 mL of solvent. The three solutions were stirred for at least 60 min before use. Then the three solutions were mixed together, in order to fabricate the mixed-cation, mixed-halide perovskite phase $Cs_{0.05}(MA_{0.15}FA_{0.85})_{0.95}PbI_{2.55}Br_{0.45}$. The resulting solution was spin-cast for 10 s at 1000 rpm and at 5000 rpm for 50 s onto a SnO_2-coated substrate. At the 40th second of the spin-coating process, 210 μL of an antisolvent (chlorobenzene) was dropped onto the substrate. Samples were transferred to a hot plate for annealing at 100 °C for 30 min, resulting in a 500 nm thick perovskite layer.

The spiro-OMeTAD solution (80 mg of spiro-OMeTAD; Lumtec), 28 μL of 4-*tert*-butylpyridine, 17.5 μL of a 520 mg mL^{-1} LiN-$(CF_3SO_2)_2N$ solution in acetonitrile, and 20 μL of a 500 mg mL^{-1} FK209 cobalt salt solution in acetonitrile were added to 1 mL of chlorobenzene; this solution was spin-cast in air at 2000 rpm for 60 s onto the perovskite film, resulting in the formation of a 200 nm thick hole transporting layer. Complete spiro-OMeTAD oxygen doping was attained by exposing the substrates to air under controlled humidity (RH = 48%) for an additional 30 min. Subsequently, the substrates were transferred to a thermal evaporator under pressure of 1.0×10^{-6} mbar, where a 100 nm Au electrode was deposited on top of the spiro-OMeTAD film. During the Au evaporation, a shadow mask was placed on each substrate, in which the overlap between the ITO and Au electrodes determined the active device area of 0.16 cm^2. Encapsulation of the devices was performed by lamination of a barrier film (R2R manufactured at the Holst Centre)[22] with a pressure-sensitive adhesive. The edge of the substrate was cleaned from the materials to ensure proper adhesion of the barrier film to the glass substrate at the edge and thereby prevent delamination and slow the side ingress of water and oxygen. The schematic illustration and photograph of the substrate containing four identical devices are shown in Supporting Information Figure S1.

Initial current density−voltage (*J*−*V*) measurements were carried out under simulated AM 1.5 G sunlight, using a MiniSunSim simulator (calibrated with c-Si cells) and a Keithley 2400 source meter. Devices were measured in both forward and reverse directions with a scan rate of 300 mV/s and then were tracked at the maximum power point (MPPT) for >120 s in order to get the stabilized value. A shadow mask of 0.09 cm^2 was used to better define the active area. The average MPPT efficiency of the devices was 16%. Typical *J*−*V* curves of fresh devices and statistics on the batch performance are shown in Figure S2. The degradation experiments were conducted with 25 cells from several batches. The data reported below represent reproducible characteristic trends.

2.2. Study of Indoor Degradation/Recovery Dynamics. Stability testing under continuous illumination (AM 1.5G, 1 kW/m^2) was performed according to ISOS-L-1 protocol standards[23] using a setup consisting of an ISOSun wide-area solar simulator with a metal halide lamp (metal halide display/optic lamp HMI from Osram) in ambient air. The ambient conditions were monitored by temperature (60 °C) and intensity sensors, and recorded periodically along with the solar cell parameters. During the continuous light exposure tests, solar cell parameters were tracked in situ via periodic *J*−*V* measurements (scanned in forward direction) every 2 min. During the dark recovery tests, light exposure of the cells took place only when the *J*−*V* measurements were conducted; otherwise, the cells were kept in the dark at room temperature between measurements. During these dark recovery periods, the solar cell parameters were tracked every 1 h for the first 8 h of measurements.

2.3. Outdoor Stability Tests. Outdoor exposure experiments were performed following the ISOS-O-1 protocol[23] in Sede Boqer, Israel (latitude, 30.8°N; longitude, 34.8°E; altitude, 475 m) during March−September 2017. The sunlight spectrum measured at noontime ±2−3 h at Sede Boqer is very close to the AM1.5G spectrum.[24] The devices were exposed to natural sunlight at open circuit during daytime (from 10:00 to 17:00) and kept in the dark in a glovebox for the rest of the time. Cells were aged under two conditions: (i) mounted on a fixed angle (30°) stand facing south and (ii) placed on a sun-tracking platform, which ensured that the dose of the impinging radiation was close to 1-sun (100 mW/cm^2) nearly throughout the entire exposure time. The dose of solar radiation during the exposure time on the tracker was typically 30−35% larger than that on the stand (see Figure S3). The comparison of the two exposure configurations can illustrate the impact of light intensity on the PSC degradation rate, as well as elucidate the adequacy of comparing the results obtained with continuous illumination (with constant 1-sun intensity) and those obtained under real operational conditions (in which a lower intensity may impinge on the cell at certain times of the day). The solar irradiance and the cell temperatures during the experiment are shown in Figure S3. No UV filtering was applied during outdoor exposure.

The *J*−*V* curves were measured twice per day, in the morning and in the evening, using a Keithley 2401 source meter under the illumination of an AAA class Oriel VeraSol LSS-7120 solar simulator (light intensity of 67 mW/cm^2). The voltage sweeps were performed in the range of −0.2 to 1.2 V in forward and reverse sweep directions at a scan rate of 40 mV/s. Only the results of reverse sweeps are shown in this work for clarity. No preconditioning was applied before the measurements.

2.4. Photoluminescence and Raman Spectroscopy Measurements. Photoluminescence (PL) and Raman spectra were measured at room temperature using a Nanofinder HE confocal spectrometer (LOTIS TII, Belarus-Japan) with a 0.1 nm (2.5 cm^{-1}) spectral resolution. A 532 nm DPSS CW laser was used as an excitation source. The excitation spot diameter was about 2 μm.

Spectral calibration was done using a built-in gas-discharge lamp providing accuracy better than 2.5 cm^{-1} (0.1 nm). For PL measurements, the sample was preconditioned for 10 min in the dark, and then 30 consecutive measurements with an acquisition time of 5 s each were

DOI: 10.1021/acsaem.7b00256
ACS Appl. Energy Mater. XXXX, XXX, XXX−XXX

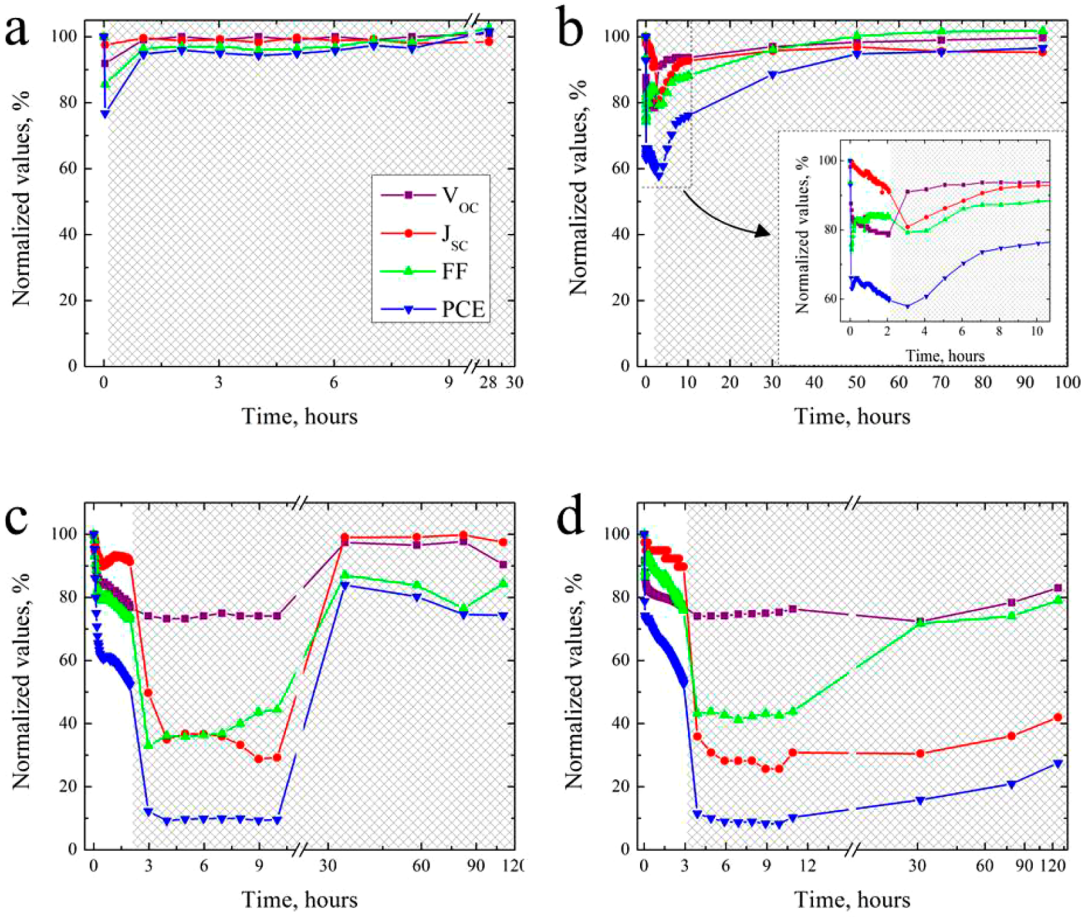

Figure 1. Evolution of PSC's PV parameters under continuous 1-sun illumination interrupted at T_{80} (a), T_{60} (b), or T_{50} (c, d) and their subsequent recovery in the dark (gray areas).

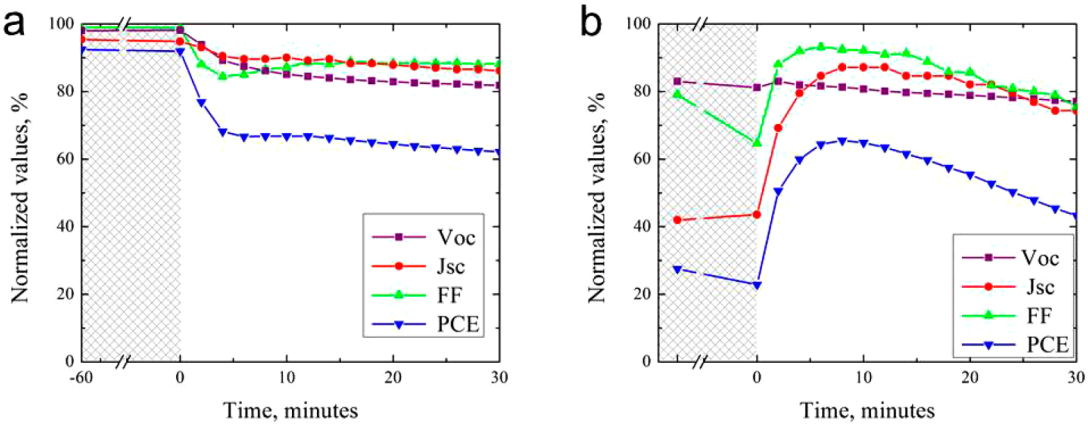

Figure 2. Evolution of PV parameters under continuous simulated 1-sun re-illumination of PSCs, following previous illumination for T_{50} and recovery in the dark (gray areas): (a) behavior of the cell whose PCE recovery in the dark reached saturation (as in Figure 1c); (b) behavior of the cell whose PCE recovery in the dark did not reach saturation (as in Figure 1d).

taken with simultaneous recording of the short-circuit current generated under the laser radiation.

3. RESULTS AND DISCUSSION

3.1. Indoor Study of Degradation/Recovery Dynamics.

The cells were divided into three batches and aged under continuous simulated 1-sun illumination until the efficiency value reached 80, 60, or 50% of the initial value (time T_{80}, T_{60}, or T_{50}, respectively). All cells were then allowed to recover in the dark. The evolution of principal PV parameters is shown in Figure 1.

Cells that degraded to 80% of their initial PCE under illumination (Figure 1a) showed almost full recovery to initial values within a few hours in the dark, in accordance with previously reported results of indoor light−darkness cycling of state-of-the-art PSCs (PCE ∼ 20%).[16] The degradation at this stage was mostly determined by the decrease in open-circuit voltage (V_{OC}) and fill factor (FF) with the minor contribution of

DOI: 10.1021/acsaem.7b00256
ACS Appl. Energy Mater. XXXX, XXX, XXX−XXX

a short-circuit current density (J_{SC}) decrease. Such *reversible* processes with full and fast recovery should not contribute to long-term deterioration of the PSC performance under day−night cycling.

The dynamics of cell performance in the dark following degradation under illumination to 50% of the initial PCE (Figure 1c,d) was found to be dramatically different from that after degradation to 80% of the initial PCE. In particular, we observed a rapid drop in J_{SC} and FF during the first 10 min of the dark storage for all cells in this batch. As a result, the PCE further decreased from 50% to ∼10% of its initial value. Corresponding $J-V$ curves showed an "s-shape" distortion (see Figure S4). This type of $J-V$ curve transformation was previously observed in organic photovoltaics[25] and PSCs.[26] For the latter, it was attributed to charge accumulation at the interface between the perovskite and transport layers or to increased surface recombination.[26]

The PCE drop at the beginning of the dark storage was followed by a slow recovery process, which either did (Figure 1c) or did not reach saturation (Figure 1d) over 5 days of measurements of different cells. It is not clear if the observed difference is qualitative or just reflects a difference in the recovery time scale. In both cases, full restoration of the initial PCE was not observed. The occurrence of *irreversible* process(es) is clearly evident even for the behavior shown in Figure 1c: the PCE restoration saturated at the level of ∼70−80% of its initial value.

Further insights into the observed dynamics related to the PCE drop after turning off the light were gained by re-illumination of these cells (Figure 2). After cell PCE recovery in the dark reached saturation (as in Figure 1c), no further light soaking improvements were observed upon re-illumination (Figure 2a). However, 1-sun re-illumination of the cell whose PCE recovery in the dark did not saturate (as in Figure 1d) resulted in a rapid PCE improvement, mostly due to increases in J_{SC} and FF, which was then followed by degradation under further illumination (Figure 2b). We note that recovery under subsequent illumination is qualitatively similar to the type II behavior observed in outdoor measurements.

Figure 1b shows the intermediate case between the degradation times of T_{80} and T_{50} described above. After the cell degraded to 60% of its initial PCE, the following combination of dynamics was observed during subsequent dark storage: fast recovery of V_{OC} (as in the T_{80} case) and initial drops in J_{SC} and FF followed by slow recovery (as in the T_{50} case, but much lower in magnitude). As a result, PCE showed slow recovery in the dark on a time scale significantly longer than one night. We consider the processes illustrated in Figure 1b,d as examples of *apparently irreversible* dynamics. We use this term since processes with such slow recovery rates would appear as irreversible under real operational day−night stressing.

3.2. Discussion of Possible Degradation Mechanisms.

3.2.1. PCE Decrease under Illumination and Recovery in the Dark. Three different mechanisms were previously suggested for reversible degradation in PSCs. Domanski et al. explained the fully reversible 10−15% PCE loss in mp-TiO_2/$MAPb(Br_xI_{1-x})_3$/spiro-OMeTAD cells by the migration of ion vacancies.[16] Both halide and cation vacancies were shown to migrate in the perovskite toward the interfaces with charge transport layers, which likely affects the charge extraction from the active layer. Nie et al. attributed the light-induced reversible J_{SC} degradation in inverted planar PSCs to the formation of metastable deep traps in the perovskite layer.[15] Hoke et al. studied photoinduced changes in the PL spectra of $MAPb(Br_xI_{1-x})_3$ perovskite films and revealed a fully reversible halide segregation into Br-rich and I-rich domains.[17]

To study reversible degradation, we simultaneously recorded changes in PL emission and J_{SC} generated by a fresh cell under 532 nm laser illumination in successive light−dark cycles (Figure 3). The integrated PL intensity, originating from radiative band-

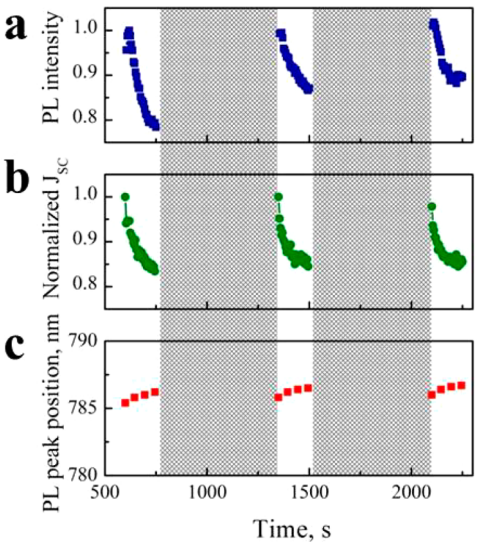

Figure 3. Time evolution of (a) the normalized wavelength integrated intensity of PL emission, (b) normalized J_{SC}, and (c) PL peak wavelength under monochromatic laser excitation (λ = 532 nm, P = 0.6 μW, d = 2 μm), upon illumination−darkness cycling of a fresh cell. We note that the laser illumination intensity is significantly higher than that of 1-sun illumination. A typical PL spectrum is shown in Figure S5.

to-band recombination in the perovskite layer, showed degradation under illumination and fast recovery in the dark. PL spectra revealed no new peak formation and only marginal (<2 nm) shifts of the main PL peak upon light−dark cycling (Figure 3c). This shift is much smaller than that observed for reversible phase segregation in mixed-halide perovskites (∼90 nm) on a similar time scale.[17] We conclude that phase segregation is not a likely explanation of our results, which can be accounted for by the low Br content (∼15%) in our perovskite layer.

Furthermore, both the J_{SC} and PL intensity decreased almost simultaneously under illumination and recovered in the dark (Figure 3a,b). Degradation caused by interfacial effects, which deteriorate charge transfer from the active layer, would decrease J_{SC} while increasing PL yield.[27] Therefore, similar reversible dynamics of these two parameters may be attributed to light-induced generation of bulk nonradiative recombination centers in the perovskite photoactive layer that may be related to the metastable traps described in ref 15 or to lattice point defects.[28] Bulk trap formation is, therefore, one of the possible mechanisms contributing to reversible degradation.

It should be noted that the PCE at the initial ($t < T_{80}$) aging stages was mostly affected by reversible V_{OC} and FF variations during light−dark cycling (Figure 1a). These may have been caused by changes in the charge extraction and electric field across the cell due to trap formation/annihilation and/or light-induced migration of ionic species in the perovskite layer.[16,18] During outdoor stability measurements, which are discussed below (section 3.3), we observed changes from morning to evening in the ratio between the V_{OC} values measured in reverse

DOI: 10.1021/acsaem.7b00256
ACS Appl. Energy Mater. XXXX, XXX, XXX−XXX

and forward scan directions, i.e., changes in the hysteresis behavior under illumination (see Figure S6). V_{OC} measured in reverse direction is higher than V_{OC} measured in forward direction, when both are measured in the morning; however this ratio is reversed in the evening measurement. As the hysteresis effect is probably linked to ion migration across the sample, the observed changes in the hysteresis behavior from morning to evening may reflect reversible ions redistribution occurring during the day, possibly resulting in reversible degradation.

3.2.2. PCE Decrease in the Dark and Recovery under Illumination. As shown above, at the later degradation stages ($t > \sim T_{50}$), rapid drops in the PCE, J_{SC}, and FF were observed immediately after turning off the light (Figure 1d). The corresponding $J-V$ curves showed an s-shape (see Figure S4) if measured without light soaking. In some cases, these parameters were restored upon re-illumination (Figure 2b).

Such dynamics have not hitherto been described in the literature, to the best of our knowledge. Though further investigation is required, we suggest the following possible scenario to explain this behavior. Shallow interfacial traps (of a different origin than the deep bulk traps described above) are generated at the later aging stages ($t > \sim T_{50}$). The traps are created under illumination and are occupied by photogenerated charge carriers that neutralize them during light illumination, and thus mitigate their effect on PSC performance. When the light is turned off, detrapping of charge carriers results in charging of these states and leads to the formation of an interfacial charge extraction barrier. This, in turn, may cause the $J-V$ curve's s-shape and the corresponding J_{SC} and FF deterioration,[29,30] as observed in our experiments. Though the traps are formed upon illumination, they significantly affect the PCE only after the light is turned off. Thus, the presence of this degradation mechanism cannot be detected in experiments commonly performed under continuous illumination, emphasizing the importance of light–dark cycling as a viable strategy for perovskite stability testing.[16]

As shown in Figure 2b, both J_{SC} and FF increased significantly within the first 10 min of re-illumination due to trap filling, before further degradation starts prevailing. According to the literature, the light soaking effect can take from minutes to hours to reach saturation.[19,20] Notably, the commonly observed light soaking effect considerably differs from our findings in the following ways: (1) in our case, it developed following ~50% PCE degradation, as opposed to being a feature of fresh devices; (2) the PCE improvement under illumination in our case was due to increases in J_{SC} and FF, as opposed to the V_{OC} increase commonly observed for light soaking;[27,31−34] and (3) the performance improvement in our case was followed by degradation under further illumination (Figure 2b). Deep traps were previously suggested to decrease V_{OC}, while shallow ones located near the charge extraction interface may induce interface charging, resulting in poor charge extraction and thus J_{SC} variations. Therefore, the hypothesis of shallow interfacial trap formation can aptly describe our observed dynamics. Interstitial ions or ion vacancies at the interface between the perovskite and transport layers are probable candidates for the microscopic origin of these shallow traps.[28,35]

In some of our experiments, after a long time in the dark, the PCE partially recovered and then saturated (Figure 1c). This slow recovery process can be attributed to trap states' *disappearance* (for instance, due to back-migration of ionic species). This suggestion is supported by the fact that no light soaking effect was observed upon re-illumination of recovered cells (Figure 2a).

3.2.3. Irreversible Degradation. Panels b and c of Figure 1 show PCE saturation without full recovery, representing irreversible long-term degradation, as was also noted in the long-term outdoor degradation of the cells (see below). Irreversible degradation mechanisms may include degradation of the perovskite photoactive layer[8,36−41] as well as transport layers and contacts,[42−44] particularly catalyzed by interlayer ion diffusion.[13,44−47] Since our indoor and outdoor experiments were conducted in air, one cannot rule out the effect of oxygen/water penetration through the encapsulation.

Commonly reported mechanisms of irreversible degradation of the perovskite layer involve its chemical decomposition upon exposure to light, humidity, and temperature[36−39] as well as irreversible trap generation[40] and ion migration to the perovskite from contact/transport layers.[41,47] The photochemical perovskite decomposition is typically accompanied by PbI_2 formation and a change of the sample color to yellow.[36−39] We did not visually observe changes of the cell color during the degradation. Raman scattering was used for more accurate PbI_2 detection (see the discussion in section 7 in the Supporting Information and Figure S7). Characteristic PbI_2 peaks were not revealed even after cell degradation to 50% of the initial PCE. Though Raman spectroscopy's sensitivity to small PbI_2 quantities can be limited, we postulate that significant perovskite decomposition was not the cause of the irreversible loss of cell performance.

3.3. Outdoor Stability Measurements and Their Correlation with Indoor Measurements. The evolution of the principal PV parameters during outdoor exposure to natural sunlight of a cell mounted on the sun-tracking platform is shown in Figure 4. Similar trends were observed for the cells mounted on the stationary stand; however, the increase in light intensity was found to increase the daily variations in PCE, especially at the late aging stages (Figure S8).

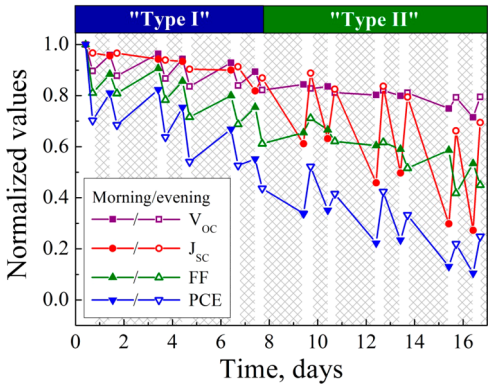

Figure 4. Evolution of the normalized values of V_{OC}, J_{SC}, FF, and PCE during outdoor exposure to natural sunlight of a PSC mounted on the sun-tracking platform. Gray areas correspond to storage time in the dark in a glovebox (16 or 40 h). The experiment with a constant storage time of 16 h is shown in Figure S9.

Both reversible and irreversible degradation processes were evident. In the first stage of the aging process ($t < 8$ days), the decrease of the PSC parameters during the day (mostly V_{OC} and FF) was partially compensated for by nighttime recovery (type I dynamics). In accordance with our recent findings,[21] this behavior leads to a significant deceleration in the long-term degradation rate as compared to degradation under constant illumination. We correlate this behavior with the one depicted in Figure 1b, i.e., with dynamics observed under constant

DOI: 10.1021/acsaem.7b00256
ACS Appl. Energy Mater. XXXX, XXX, XXX−XXX

illumination at $t < T_{50}$, with degradation governed by the decrease in V_{OC} and FF with a minor contribution by the decrease in J_{SC}, and significant recovery in the dark. Full recovery was not observed in the outdoor test. This can be explained by the fact that, during the first day of exposure, the PCE decreased to ~70% of its initial value. This corresponds to the degradation stage under continuous illumination at which full recovery within 16 h (one night) is not possible due to irreversible and/or "apparently irreversible" processes (with recovery time longer than one night, Figure 1b). Increased dark storage time from 16 to 40 h did not result in a significantly higher degree of recovery (see Figure 4).

At later degradation stages (t > 8 days), the diurnal kinetics of PCE changed to that of type II in which the PCE decreased during the nighttime and increased during the daytime, mostly following variations in J_{SC} (see also Figure S10 for hourly resolved parameters evolution during a given day, before and after the change in diurnal dynamics). This was accompanied by the appearance of the s-shape in the $J-V$ curves measured in the forward direction in the morning, i.e., after dark storage (see Figure S4). This behavior was observed after the PCE decreased to less than 50% of its initial value, roughly corresponding to the onset of dynamics including a sharp PCE decrease immediately after light turn-off in the indoor experiments (Figure 1d). As both are characterized by a decrease in the PCE in the dark and its increase under subsequent illumination, we suggest that they are caused by similar degradation mechanism(s).

We traced the evolution of the performance during dark storage of the cells that were severely degraded outdoors (to 30–40% of their initial PCE) for 3 months and found that full restoration did not occur (Figure S9), clearly proving the presence of irreversible degradation processes.

A combined analysis of the results shown in Figures 1, 2, and 4 allows us to suggest the following scenario for cell degradation under operational conditions. At the very early stages of aging ($t \leq T_{80}$ in our case), only reversible degradation takes place. Then, at $t > T_{60}$, in parallel with the reversible degradation, irreversible degradation processes kick in. Finally, at $t \sim T_{50}$, when the diurnal dynamics of type I changes to that of type II, these processes begin to be accompanied by a third type of unique dynamics, which includes further degradation after light turn-off and subsequent PCE improvement under light soaking.

4. SUMMARY AND CONCLUSIONS

We studied the stability of PSCs with a structure of ITO/SnO_2/$Cs_{0.05}(MA_{0.15}FA_{0.85})_{0.95}PbI_{2.55}Br_{0.45}$/spiro-OMeTAD/Au in realistic outdoor conditions as well as the kinetics of their PCE recovery in the dark after aging by continuous simulated sunlight. We observed qualitatively different dark recovery kinetics at different aging stages. Fully reversible degradation was observed at the early stage ($t \leq T_{80}$). This can be attributed to metastable defect formation or reversible ion redistribution under illumination. A completely different restoration dynamics was revealed after $t \geq T_{50}$: a rapid decrease in J_{SC} and FF upon light turn-off was noticed at this stage, which was followed by a slow, incomplete recovery. Before the recovery reached saturation, FF and J_{SC} showed rapid increases under further illumination. A charge extraction barrier formed by interfacial shallow traps is suggested as a possible underlying mechanism. In the interim regime, i.e., following PCE degradation by 20–50%, recovery is possible but the recovery time exceeds one night; thus, it will appear (partially) irreversible in the day–night cycle.

Measurements of diurnal PCE changes under real operational conditions showed that for fresh cells, PCE decreased under illumination and partially recovered during the night, while the opposite diurnal dynamics were found after significant degradation. The interplay of degradation mechanisms with different recovery dynamics discussed above can explain the observed changes, connecting the indoor and outdoor measurements.

We have demonstrated that the study of the dynamics of processes occurring in the dark, as well as under light exposure, contributes to understanding PSC degradation mechanisms. Illumination by light–darkness cycles should be included in experimental protocols for the assessment of PSCs' long-term stability.

■ ASSOCIATED CONTENT

Supporting Information

The Supporting Information is available free of charge on the ACS Publications website at DOI: 10.1021/acsaem.7b00256.

Schematic illustrations and photograph of studied cells, their initial performance, weather conditions during the outdoor stability testing, examples of measured $J-V$ curves, photoluminescence and Raman spectra, and additional results of outdoor stability measurements (PDF)

■ AUTHOR INFORMATION

Corresponding Author

*E-mail: keugene@bgu.ac.il.

ORCID

Mark V. Khenkin: 0000-0001-9201-0238
Iris Visoly-Fisher: 0000-0001-6058-4712
Yulia Galagan: 0000-0002-3637-5459
Francesco Di Giacomo: 0000-0002-2489-5385
Bhushan Ramesh Patil: 0000-0001-7249-6330
Horst-Günter Rubahn: 0000-0002-3606-5653
Morten Madsen: 0000-0001-6503-0479
Alexander V. Mazanik: 0000-0002-4725-0969
Eugene A. Katz: 0000-0001-6151-1603

Notes

The authors declare no competing financial interest.

■ ACKNOWLEDGMENTS

This work was supported by the European Commission's StableNextSol COST Action MP1307. The research was funded in part by Israel's Ministry of National Infrastructures, Water and Energy Resources (Grant No. 0399202/215-11-037) and by the Adelis Foundation. E.A.K. and M.V.K. also thank the United States–Israel Binational Science Foundation. A.V.M. is grateful to the Belarusian Republican Foundation for Fundamental Research (Grant No. F16MS-015). Y.G. appreciates support by Solliance, a partnership of R&D organizations from The Netherlands, Belgium, and Germany working in thin film photovoltaic solar energy. G.S., M.M., and H.-G.R. acknowledge funding from the European Union Seventh Framework Programme under Grant Agreement No. 607232 (THINFACE). V.T. acknowledges "Det Frie Forskningsråd", DFF FTP, for funding of the project Stabil-O.

DOI: 10.1021/acsaem.7b00256
ACS Appl. Energy Mater. XXXX, XXX, XXX–XXX

REFERENCES

(1) Yang, W. S.; Park, B.-W.; Jung, E. H.; Jeon, N. J.; Kim, Y. C.; Lee, D. U.; Shin, S. S.; Seo, J.; Kim, E. K.; Noh, J. H.; Seok, S. I. Iodide Management in Formamidinium-Lead-Halide–based Perovskite Layers for Efficient Solar Cells. *Science* **2017**, *356*, 1376–1379.

(2) Kim, J.; Yun, J. S.; Cho, Y.; Lee, D. S.; Wilkinson, B.; Soufiani, A. M.; Deng, X.; Zheng, J.; Shi, A.; Lim, S.; Chen, S.; Hameiri, Z.; Zhang, M.; Lau, C. F. J.; Huang, S.; Green, M. A.; Ho-Baillie, A. W. Y. Overcoming the Challenges of Large-Area High-Efficiency Perovskite Solar Cells. *ACS Energy Lett.* **2017**, *2*, 1978–1984.

(3) Di Giacomo, F.; Shanmugam, S.; Fledderus, H.; Bruijnaers, B. J.; Verhees, W. J. H.; Dorenkamper, M. S.; Veenstra, S. C.; Qiu, W.; Gehlhaar, R.; Merckx, T.; Aernouts, T.; Andriessen, R.; Galagan, Y. Up-Scalable Sheet-to-Sheet Production of High Efficiency Perovskite Module and Solar Cells on 6-in. Substrate Using Slot Die Coating. *Sol. Energy Mater. Sol. Cells* **2017**, DOI: 10.1016/j.solmat.2017.11.010, (in press).

(4) Divitini, G.; Cacovich, S.; Matteocci, F.; Cinà, L.; Di Carlo, A.; Ducati, C. *In Situ* Observation of Heat-Induced Degradation of Perovskite Solar Cells. *Nat. Energy* **2016**, *1*, 15012.

(5) Zhao, X.; Kim, H.-S.; Seo, J.-Y.; Park, N.-G. Effect of Selective Contacts on the Thermal Stability of Perovskite Solar Cells. *ACS Appl. Mater. Interfaces* **2017**, *9*, 7148–7153.

(6) Kim, N.-K.; Min, Y. H.; Noh, S.; Cho, E.; Jeong, G.; Joo, M.; Ahn, S.-W.; Lee, J. S.; Kim, S.; Ihm, K.; Ahn, H.; Kang, Y.; Lee, H.-S.; Kim, D. Investigation of Thermally Induced Degradation in CH 3 NH 3 PbI 3 Perovskite Solar Cells Using In-Situ Synchrotron Radiation Analysis. *Sci. Rep.* **2017**, *7*, 4645.

(7) Gottesman, R.; Zaban, A. Perovskites for Photovoltaics in the Spotlight: Photoinduced Physical Changes and Their Implications. *Acc. Chem. Res.* **2016**, *49*, 320–329.

(8) Leijtens, T.; Eperon, G. E.; Pathak, S.; Abate, A.; Lee, M. M.; Snaith, H. J. Overcoming Ultraviolet Light Instability of Sensitized TiO_2 with Meso-Superstructured Organometal Tri-halide Perovskite Solar Cells. *Nat. Commun.* **2013**, *4*, 3885.

(9) Lee, S.-W.; Kim, S.; Bae, S.; Cho, K.; Chung, T.; Mundt, L. E.; Lee, S.; Park, S.; Park, H.; Schubert, M. C.; Glunz, S. W.; Ko, Y.; Jun, Y.; Kang, Y.; Lee, H.-S.; Kim, D. UV Degradation and Recovery of Perovskite Solar Cells. *Sci. Rep.* **2016**, *6*, 38150.

(10) Bae, S.; Kim, S.; Lee, S.-W.; Cho, K. J.; Park, S.; Lee, S.; Kang, Y.; Lee, H.-S.; Kim, D. Electric-Field-Induced Degradation of Methylammonium Lead Iodide Perovskite Solar Cells. *J. Phys. Chem. Lett.* **2016**, *7*, 3091–3096.

(11) Yadav, P.; Prochowicz, D.; Alharbi, E. A.; Zakeeruddin, S. M.; Grätzel, M. Intrinsic and Interfacial Kinetics of Perovskite Solar Cells under Photo and Bias-Induced Degradation and Recovery. *J. Mater. Chem. C* **2017**, *5*, 7799–7805.

(12) Yang, J.; Siempelkamp, B. D.; Liu, D.; Kelly, T. L. Investigation of CH3NH3PbI3 Degradation Rates and Mechanisms in Controlled Humidity Environments Using in Situ Techniques. *ACS Nano* **2015**, *9*, 1955–1963.

(13) Reyna, Y.; Salado, M.; Kazim, S.; Pérez-Tomas, A.; Ahmad, S.; Lira-Cantu, M. Performance and Stability of Mixed FAPbI3(0.85)-MAPbBr3(0.15) Halide Perovskite Solar Cells under Outdoor Conditions and the Effect of Low Light Irradiation. *Nano Energy* **2016**, *30*, 570–579.

(14) Li, X.; Tschumi, M.; Han, H.; Babkair, S. S.; Alzubaydi, R. A.; Ansari, A. A.; Habib, S. S.; Nazeeruddin, M. K.; Zakeeruddin, S. M.; Grätzel, M. Outdoor Performance and Stability under Elevated Temperatures and Long-Term Light Soaking of Triple-Layer Mesoporous Perovskite Photovoltaics. *Energy Technol.* **2015**, *3*, 551–555.

(15) Nie, W.; Blancon, J.-C.; Neukirch, A. J.; Appavoo, K.; Tsai, H.; Chhowalla, M.; Alam, M. A.; Sfeir, M. Y.; Katan, C.; Even, J.; Tretiak, S.; Crochet, J. J.; Gupta, G.; Mohite, A. D. Light-Activated Photocurrent Degradation and Self-Healing in Perovskite Solar Cells. *Nat. Commun.* **2016**, *7*, 11574.

(16) Domanski, K.; Roose, B.; Matsui, T.; Saliba, M.; Turren-Cruz, S.-H.; Correa-Baena, J.-P.; Carmona, C. R.; Richardson, G.; Foster, J. M.; De Angelis, F.; Ball, J. M.; Petrozza, A.; Mine, N.; Nazeeruddin, M. K.; Tress, W.; Grätzel, M.; Steiner, U.; Hagfeldt, A.; Abate, A. Migration of Cations Induces Reversible Performance Losses over Day/Night Cycling in Perovskite Solar Cells. *Energy Environ. Sci.* **2017**, *10*, 604–613.

(17) Hoke, E. T.; Slotcavage, D. J.; Dohner, E. R.; Bowring, A. R.; Karunadasa, H. I.; McGehee, M. D. Reversible Photo-Induced Trap Formation in Mixed-Halide Hybrid Perovskites for Photovoltaics. *Chem. Sci.* **2015**, *6*, 613–617.

(18) Bag, M.; Renna, L. A.; Adhikari, R. Y.; Karak, S.; Liu, F.; Lahti, P. M.; Russell, T. P.; Tuominen, M. T.; Venkataraman, D. Kinetics of Ion Transport in Perovskite Active Layers and Its Implications for Active Layer Stability. *J. Am. Chem. Soc.* **2015**, *137*, 13130–13137.

(19) Huang, F.; Jiang, L.; Pascoe, A. R.; Yan, Y.; Bach, U.; Spiccia, L.; Cheng, Y.-B. Fatigue Behavior of Planar CH3NH3PbI3 Perovskite Solar Cells Revealed by Light on/off Diurnal Cycling. *Nano Energy* **2016**, *27*, 509–514.

(20) Liu, F.; Dong, Q.; Wong, M. K.; Djurišić, A. B.; Ng, A.; Ren, Z.; Shen, Q.; Surya, C.; Chan, W. K.; Wang, J.; Ng, A. M. C.; Liao, C.; Li, H.; Shih, K.; Wei, C.; Su, H.; Dai, J. Is Excess PbI2 Beneficial for Perovskite Solar Cell Performance? *Adv. Energy Mater.* **2016**, *6*, 1502206.

(21) Khenkin, M. V.; Anoop, K. M.; Visoly-Fisher, I.; Galagan, Y.; Di Giacomo, F.; Patil, B. R.; Sherafatipour, G.; Turkovic, V.; Madsen, M.; Merckx, T.; Uytterhoeven, G.; Bastos, J. P. A.; Aernouts, T.; Brunetti, F.; Lira-Cantu, M.; Katz, E. A. Reconsidering Figures of Merit for the Performance and Stability of Perovskite Photovoltaics. Submitted for publication.

(22) Van de Weijer, P.; Bouten, P. C. P.; Unnikrishnan, S.; Akkerman, H. B.; Michels, J. J.; van Mol, T. M. B. High-Performance Thin-Film Encapsulation for Organic Light-Emitting Diodes. *Org. Electron.* **2017**, *44*, 94–98.

(23) Reese, M. O.; Gevorgyan, S. A.; Jørgensen, M.; Bundgaard, E.; Kurtz, S. R.; Ginley, D. S.; Olson, D. C.; Lloyd, M. T.; Morvillo, P.; Katz, E. A.; Elschner, A.; Haillant, O.; Currier, T. R.; Shrotriya, V.; Hermenau, M.; Riede, M.; Kirov, K. R.; Trimmel, G.; Rath, T.; Inganäs, O.; Zhang, F.; Andersson, M.; Tvingstedt, K.; Lira-Cantu, M.; Laird, D.; McGuiness, C.; Gowrisanker, S. J.; Pannone, M.; Xiao, M.; Hauch, J.; Steim, R.; DeLongchamp, D. M.; Rösch, R.; Hoppe, H.; Espinosa, N.; Urbina, A.; Yaman-Uzunoglu, G.; Bonekamp, J.-B.; van Breemen, A. J. J. M.; Girotto, C.; Voroshazi, E.; Krebs, F. C. Consensus Stability Testing Protocols for Organic Photovoltaic Materials and Devices. *Sol. Energy Mater. Sol. Cells* **2011**, *95*, 1253–1267.

(24) Inasaridze, L. N.; Shames, A. I.; Martynov, I. V.; Li, B.; Mumyatov, A. V.; Susarova, D. K.; Katz, E. A.; Troshin, P. A. Light-Induced Generation of Free Radicals by Fullerene Derivatives: An Important Degradation Pathway in Organic Photovoltaics? *J. Mater. Chem. A* **2017**, *5*, 8044–8050.

(25) Finck, B. Y.; Schwartz, B. J. Understanding the Origin of the S-Curve in Conjugated Polymer/Fullerene Photovoltaics from Drift-Diffusion Simulations. *Appl. Phys. Lett.* **2013**, *103*, 053306.

(26) Jacobs, D. A.; Wu, Y.; Shen, H.; Barugkin, C.; Beck, F. J.; White, T. P.; Weber, K.; Catchpole, K. R. Hysteresis Phenomena in Perovskite Solar Cells: The Many and Varied Effects of Ionic Accumulation. *Phys. Chem. Chem. Phys.* **2017**, *19*, 3094–3103.

(27) Zhao, C.; Chen, B.; Qiao, X.; Luan, L.; Lu, K.; Hu, B. Revealing Underlying Processes Involved in Light Soaking Effects and Hysteresis Phenomena in Perovskite Solar Cells. *Adv. Energy Mater.* **2015**, *5*, 1500279.

(28) Yin, W.-J.; Shi, T.; Yan, Y. Unusual Defect Physics in CH3NH3PbI3 Perovskite Solar Cell Absorber. *Appl. Phys. Lett.* **2014**, *104*, 063903.

(29) Van Reenen, S.; Kemerink, M.; Snaith, H. J. Modeling Anomalous Hysteresis in Perovskite Solar Cells. *J. Phys. Chem. Lett.* **2015**, *6*, 3808–3814.

(30) Shao, S.; Liu, J.; Fang, H.-H.; Qiu, L.; ten Brink, G. H.; Hummelen, J. C.; Koster, L. J. A.; Loi, M. A. Efficient Perovskite Solar Cells over a Broad Temperature Window: The Role of the Charge Carrier Extraction. *Adv. Energy Mater.* **2017**, *7*, 1701305.

DOI: 10.1021/acsaem.7b00256
ACS Appl. Energy Mater. XXXX, XXX, XXX–XXX

(31) Shao, S.; Abdu-Aguye, M.; Sherkar, T. S.; Fang, H.-H.; Adjokatse, S.; ten Brink, G.; Kooi, B. J.; Koster, L. J. A.; Loi, M. A. The Effect of the Microstructure on Trap-Assisted Recombination and Light Soaking Phenomenon in Hybrid Perovskite Solar Cells. *Adv. Funct. Mater.* **2016**, *26*, 8094−8102.
(32) Peng, J.; Sun, Y.; Chen, Y.; Yao, Y.; Liang, Z. Light and Thermally Induced Evolutional Charge Transport in CH3NH3PbI3 Perovskite Solar Cells. *ACS Energy Lett.* **2016**, *1*, 1000−1006.
(33) Lv, S.; Pang, S.; Zhou, Y.; Padture, N. P.; Hu, H.; Wang, L.; Zhou, X.; Zhu, H.; Zhang, L.; Huang, C.; Cui, G. One-Step, Solution-Processed Formamidinium Lead Trihalide (FAPbI(3−x)Clx) for Mesoscopic Perovskite−polymer Solar Cells. *Phys. Chem. Chem. Phys.* **2014**, *16*, 19206−19211.
(34) Liu, C.; Fan, J.; Zhang, X.; Shen, Y.; Yang, L.; Mai, Y. Hysteretic Behavior upon Light Soaking in Perovskite Solar Cells Prepared via Modified Vapor-Assisted Solution Process. *ACS Appl. Mater. Interfaces* **2015**, *7*, 9066−9071.
(35) Du, M. H. Efficient Carrier Transport in Halide Perovskites: Theoretical Perspectives. *J. Mater. Chem. A* **2014**, *2*, 9091−9098.
(36) Noh, J. H.; Im, S. H.; Heo, J. H.; Mandal, T. N.; Seok, S. I. Chemical Management for Colorful, Efficient, and Stable Inorganic−Organic Hybrid Nanostructured Solar Cells. *Nano Lett.* **2013**, *13*, 1764−1769.
(37) Niu, G.; Li, W.; Meng, F.; Wang, L.; Dong, H.; Qiu, Y. Study on the Stability of CH3NH3PbI3 Films and the Effect of Post-Modification by Aluminum Oxide in All-Solid-State Hybrid Solar Cells. *J. Mater. Chem. A* **2014**, *2*, 705−710.
(38) Misra, R. K.; Aharon, S.; Li, B.; Mogilyansky, D.; Visoly-Fisher, I.; Etgar, L.; Katz, E. A. Temperature- and Component-Dependent Degradation of Perovskite Photovoltaic Materials under Concentrated Sunlight. *J. Phys. Chem. Lett.* **2015**, *6*, 326−330.
(39) Misra, R. K.; Ciammaruchi, L.; Aharon, S.; Mogilyansky, D.; Etgar, L.; Visoly-Fisher, I.; Katz, E. A. Effect of Halide Composition on the Photochemical Stability of Perovskite Photovoltaic Materials. *ChemSusChem* **2016**, *9*, 2572−2577.
(40) Song, D.; Ji, J.; Li, Y.; Li, G.; Li, M.; Wang, T.; Wei, D.; Cui, P.; He, Y.; Mbengue, J. M. Degradation of Organometallic Perovskite Solar Cells Induced by Trap States. *Appl. Phys. Lett.* **2016**, *108*, 093901.
(41) Domanski, K.; Correa-Baena, J.-P.; Mine, N.; Nazeeruddin, M. K.; Abate, A.; Saliba, M.; Tress, W.; Hagfeldt, A.; Grätzel, M. Not All That Glitters Is Gold: Metal-Migration-Induced Degradation in Perovskite Solar Cells. *ACS Nano* **2016**, *10*, 6306−6314.
(42) Abate, A.; Paek, S.; Giordano, F.; Correa-Baena, J.-P.; Saliba, M.; Gao, P.; Matsui, T.; Ko, J.; Zakeeruddin, S. M.; Dahmen, K. H.; Hagfeldt, A.; Grätzel, M.; Nazeeruddin, M. K. Silolothiophene-Linked Triphenylamines as Stable Hole Transporting Materials for High Efficiency Perovskite Solar Cells. *Energy Environ. Sci.* **2015**, *8*, 2946−2953.
(43) Guarnera, S.; Abate, A.; Zhang, W.; Foster, J. M.; Richardson, G.; Petrozza, A.; Snaith, H. J. Improving the Long-Term Stability of Perovskite Solar Cells with a Porous Al2O3 Buffer Layer. *J. Phys. Chem. Lett.* **2015**, *6*, 432−437.
(44) Zhao, Y.; Zhou, W.; Tan, H.; Fu, R.; Li, Q.; Lin, F.; Yu, D.; Walters, G.; Sargent, E. H.; Zhao, Q. Mobile-Ion-Induced Degradation of Organic Hole-Selective Layers in Perovskite Solar Cells. *J. Phys. Chem. C* **2017**, *121*, 14517−14523.
(45) Cacovich, S.; Ciná, L.; Matteocci, F.; Divitini, G.; Midgley, P. A.; Di Carlo, A.; Ducati, C. Gold and Iodine Diffusion in Large Area Perovskite Solar Cells under Illumination. *Nanoscale* **2017**, *9*, 4700−4706.
(46) Akbulatov, A. F.; Frolova, L. A.; Griffin, M. P.; Gearba, I. R.; Dolocan, A.; Vanden Bout, D. A.; Tsarev, S.; Katz, E. A.; Shestakov, A. F.; Stevenson, K. J.; Troshin, P. A. Effect of Electron-Transport Material on Light-Induced Degradation of Inverted Planar Junction Perovskite Solar Cells. *Adv. Energy Mater.* **2017**, *7*, 1700476.
(47) Li, Z.; Xiao, C.; Yang, Y.; Harvey, S. P.; Kim, D. H.; Christians, J. A.; Yang, M.; Schulz, P.; Nanayakkara, S. U.; Jiang, C.-S.; Luther, J. M.; Berry, J. J.; Beard, M. C.; Al-Jassim, M. M.; Zhu, K. Extrinsic Ion Migration in Perovskite Solar Cells. *Energy Environ. Sci.* **2017**, *10*, 1234−1242.

DOI: 10.1021/acsaem.7b00256
ACS Appl. Energy Mater. XXXX, XXX, XXX−XXX